Dipole and Quadrupole Solitons in Optically Induced Two-Dimensional Photonic Lattices: Theory and Experiment

By Jianke Yang, Igor Makasyuk, Anna Bezryadina, and Zhigang Chen

Dipole and quadrupole solitons in a two-dimensional photorefractive optical lattice are investigated both theoretically and experimentally. It is shown theoretically that out-of-phase dipole solitons and quadrupole solitons exist and are linearly stable in the intermediate-intensity regime. In-phase dipole and quadrupole solitons, however, are always linearly unstable, but their instabilities are rather weak in the low-intensity regime. Experimentally, both types of dipole solitons are observed, and the experimental results agree qualitatively with the theoretical predictions. In addition, we have observed the anisotropic effect of the photorefractive crystal in the dipole-soliton formation.

1. Introduction

Light propagation in a nonlinear medium is a fascinating subject in physics. In free space, light has a natural tendency to broaden due to diffraction. However, the nonlinear effect in the medium can cause the light to self-focus. When this self-focusing effect counteracts diffraction, light can form an optical spatial soliton [1]. In one dimension (1D), solitons in a homogeneous Kerr slab

Address for correspondence: J. Yang, Department of Mathematics and Statistics, University of Vermont, 16 Colchester Avenue, Burlington, VT 05401-1455; e-mail: jyang@emba.uvm.edu

STUDIES IN APPLIED MATHEMATICS 113:389–412

Published by Blackwell Publishing, 350 Main Street, Malden, MA 02148, USA, and 9600 Garsington Road, Oxford, OX4 2DQ, UK.

waveguide (where nonlinearity is cubic) exist and are stable [2, 3], and they have been observed in experiments [4]. However, in an ideal homogeneous Kerr medium, 2D solitons suffer critical collapse [5], and thus have never been observed. Even 1D solitons experience transverse modulational instability in a 2D bulk Kerr medium [6]. Photorefractive materials [7], on the other hand, were found to exhibit the self-focusing effect, but the nonlinearity is saturable, in contrast to traditional Kerr nonlinearity. Subsequent studies revealed that the saturable nonlinearity suppresses the critical collapse in two dimensions, thus photorefractive solitons are stable in both one and two dimensions [8, 9], and have subsequently been observed in experiments [10, 11].

Recently, light propagation in periodic photonic lattices is stirring a lot of interest due to their novel physics, light-routing applications as well as connections to photonic crystals [12, 13]. The linear propagation of light in a periodic lattice is already a nontrivial phenomena. Indeed, the periodic lattice creates a bandgap structure in the propagation-constant space. If the incoming light lies within a band, it could transmit through. However if the light lies inside a bandgap, its propagation would be evanescent instead [14]. In addition, linear light propagation inside a periodic lattice exhibits interesting discrete-diffraction patterns that have no counterpart in the homogeneous medium. On the other hand, if the nonlinear effects of the waveguide are significant, light could self-focus into various lattice-soliton structures inside the bandgap. These lattice solitons have distinctive geometric structures (such as the existence of side lobes surrounding the main hump). Their stability properties also exhibit novel features that are absent in the homogeneous medium. So far, fundamental and vortex lattice solitons as well as vector lattice solitons have been reported both theoretically and experimentally in both one and two dimensions [15–26]. Dipole solitons in 1D systems [17, 27, 28] as well as in 2D discrete nonlinear Schrödinger equations [29] have also been studied.

In this paper, we report theoretical and experimental results on dipole and quadrupole solitons in a 2D photorefractive lattice. These solitons can be either in-phase (IP) or out-of-phase (OOP) between their humps. Moreover, the dipole solitons can be located in two closest diagonal lattice sites (i.e., 45° relative to the principal axes) or two closest nondiagonal lattice sites (i.e., along the principal axes) in a 2D square photonic lattice. In the absence of the lattice, these solitons cannot exist due to the repulsive or attractive forces between the humps. However, in the presence of the lattice, the lattice creates an optical waveguide that could trap the individual humps against attraction or repulsion, leading to the formation of dipole and quadrupole solitons. Our stability analysis shows that OOP dipole and quadrupole solitons are linearly unstable at high- and low-intensity regimes, but are stable at the intermediate-intensity regime. On the other hand, IP dipole and quadrupole solitons are always linearly unstable. However, for both IP and OOP solitons at low intensities,

their instabilities are rather weak. Experimentally, we have observed both IP and OOP dipole solitons at high voltages. The experimental results are in good agreement with the theoretical results.

Let us consider laser beam propagation in a photorefractive crystal with a 2D optically induced photonic lattice (see Figure 5). The laser beam is launched along the extraordinary axis of the crystal to take advantage of the large electrooptic coefficient (i.e., strong nonlinearity) along this polarization. On the other hand, the lattice beam goes through an amplitude mask to create a periodic amplitude modulation, and is launched along the ordinary axis of the crystal. Due to the small electrooptic coefficient along this axis as well as the fact that the lattice beam is made partially incoherent (to suppress modulational instability), a stable and uniform lattice field can then be established inside the crystal [30]. The theoretical model for a laser beam propagating in this lattice field can be derived from the Maxwell equations. Taking the paraxial approximation and neglecting the anisotropic properties of the crystal, the theoretical model becomes (after nondimensionalization) [16]

$$iU_z + U_{xx} + U_{yy} - \frac{E_0}{1 + I_l + |U|^2} U = 0, \tag{1}$$

where U is the slowly varying amplitude of the probe beam normalized by the dark irradiance of the crystal I_d, and

$$I_l = I_0 \sin^2 \frac{x+y}{\sqrt{2}} \sin^2 \frac{x-y}{\sqrt{2}}$$

is a square-lattice intensity function (in units of I_d) that closely resembles the lattice in our experiments. Here I_0 is the lattice peak intensity, z is the propagation distance (in units of $2k_1 D^2/\pi^2$), (x, y) are transverse distances (in units of D/π), E_0 is the applied DC field voltage [in units of $\pi^2/(k_0^2 n_e^4 D^2 r_{33})$], D is the lattice spacing, $k_0 = 2\pi/\lambda_0$ is the wavenumber of the laser in the vacuum, (λ_0 is the wavelength), n_e is the refractive index along the extraordinary axis, $k_1 = k_0 n_e$, and r_{33} is the electrooptic coefficient for the extraordinary polarization. Consistent with our experiment, we choose the lattice intensity $I_0 = 3I_d$. In addition, we choose other physical parameters as

$$D = 20\,\mu\text{m}, \quad \lambda_0 = 0.5\,\mu\text{m}, \quad n_e = 2.3, \quad r_{33} = 280\,\text{pm/V}.$$

Thus, in this paper, one x or y unit corresponds to 6.4 μm, one z unit corresponds to 2.3 mm, and one E_0 unit corresponds to 20 V/mm in physical units.

Stationary dipole or quadrupole solitons in the model equation (1) are sought in the form $U = u(x, y)e^{-i\mu z}$, where u is a *real-valued* function, and μ is the propagation constant. Then $u(x, y)$ satisfies the nonlinear equation

$$u_{xx} + u_{yy} + \left(\mu - \frac{E_0}{1 + I_l + u^2}\right) u = 0. \tag{2}$$

The solution u can be determined by a modification of the Fourier iteration method proposed in [31] as follows. First we separate the linear and nonlinear terms in Equation (2) and put them on two different sides

$$u_{xx} + u_{yy} + (\mu - E_0 + P)u = Q, \tag{3}$$

where

$$P \equiv \frac{E_0 I_l}{1 + |u|^2 + I_l}, \quad Q \equiv -\frac{E_0 |u|^2 u}{1 + |u|^2 + I_l}.$$

Then we take the Fourier transform to Equation (3), and get

$$\hat{u} = \frac{1}{|\mathbf{k}|^2 - \mu + E_0} \{\mathcal{F}(Pu) - \mathcal{F}(Q)\}. \tag{4}$$

Here $\mathcal{F}(\cdot)$ is the 2D Fourier transform, and $\hat{u} = \mathcal{F}(u)$. Straightforward iteration of Equation (4) does not converge in general. The key idea in [30] is to introduce a stabilizing factor to Equation (4). Define

$$\alpha = \int \left\{|\mathbf{k}|^2 - \mu + E_0)\hat{u} - \mathcal{F}(Pu)\right\}\hat{u}^* \, d\mathbf{k}, \quad \beta = -\int \mathcal{F}(Q)\hat{u}^* \, d\mathbf{k},$$

where the superscript "*" represents complex conjugation, then we construct the following iteration equation:

$$\hat{u}_{m+1} = \frac{1}{|\mathbf{k}|^2 - \mu + E_0} \left\{ \left(\frac{\alpha_m}{\beta_m}\right)^{1/2} \mathcal{F}(P_m u_m) - \left(\frac{\alpha_m}{\beta_m}\right)^{3/2} \mathcal{F}(Q_m) \right\}. \tag{5}$$

With this scheme, we have found various dipole and quadrupole solitons to be reported.

Linear stability of these dipole and quadrupole solitons is clearly an important issue. This question can be analyzed as follows. We first perturb these solitons as $U = e^{-\mu z}\{u(x, y) + \tilde{U}(x, y, z)\}$, where $u(x, y)$ is the dipole or quadrupole soliton, and $\tilde{U} \ll 1$ is the infinitesimal perturbation. When this perturbed solution is substituted into Equation (1), the linearized equation for $\tilde{U}$ is

$$i\tilde{U}_z + \mu\tilde{U} + \tilde{U}_{xx} + \tilde{U}_{yy} - \frac{E_0\left[(1 + I_l)\tilde{U} - u^2\tilde{U}^*\right]}{\left(1 + I_l + u^2\right)^2} = 0, \tag{6}$$

Starting with a random-noise initial condition, we simulated this linearized equation for long distances (hundreds of z units). If the solution grows exponentially, then the underlying dipole soliton would be linearly unstable, the exponential constant would be the unstable eigenvalue, and the real part of this eigenvalue would be the growth rate of infinitesimal perturbations.

2. Dipole solitons in two closest diagonal lattice sites

In this section, we report dipole solitons whose two lobes are located in two diagonal lattice sites in a 2D square lattice. These lobes can have the same phase, or have π-phase difference. The resulting solitons are called *diagonal IP* and *OOP dipole solitons*, respectively. For these studies, the lattice's principal axes are oriented diagonally, so the dipole solitons can be oriented in either the vertical or horizontal direction (see Figures 1, 6, and 7 for the lattice and dipole orientations).

2.1. Diagonal OOP dipole solitons

We have found diagonal OOP dipole solitons in a large region of the voltage (E_0) and propagation constant (μ) space. These solitons have two main humps. The phases of the upper-half field are zero, and those of the lower-half field are π. At $E_0 = 6$, these solitons exist when $1.455 < \mu < 3.51$, or equivalently when their peak intensities I_p are in the range $0.94 < I_p < 15.7$. These solitons are displayed in Figure 1. Here the upper row shows three diagonal OOP dipole solitons with peak intensities 12, 3, and 1, respectively (the corresponding propagation constants μ are 1.80, 3.11, and 3.50). Notice that at high intensities, the two humps of the dipoles do not reside at the centers of two diagonal lattice sites (see Figure 1(a)). Instead, they reside at the outskirts of diagonal lattice sites, so that the distance between them is considerably larger than the diagonal lattice spacing. This can be understood intuitively as follows. Since when two beams are OOP and are with high intensities, the two humps repel each other strongly, but the trapping force of the lattice-induced waveguide remains about the same (since the lattice intensity is not changed). As the propagation distance increases, the distance between the two humps increases, so the repelling force between then decreases. When the distance is large enough that the repelling force balances the trapping force, a new equilibrium of dipole solitons is then reached. When the intensity of the dipole soliton is moderate, the two humps of the dipole do reside at the centers of diagonal lattice sites (see Figure 1(b)). In addition, the soliton is quite localized. If the intensity is low, however, the soliton becomes less localized, and the intensity field spreads to more lattice sites in a manner as shown in Figure 1(c). In all these solitons, the field intensity between the two main humps is very low due to the destructive interference of the two main humps. We have also obtained the power and peak-intensity diagrams for these solitons, which are shown in Figure 1. We see that the intensity is a decreasing functions of the propagation constant μ. The power also decreases for most values of μ ($\mu < 3.49$), but starts to increase in the tiny interval $3.49 < \mu < 3.51$. Since these solitons disappear when $\mu > 3.51$, this short interval of increasing power is hardly visible in Figure 1(e). From the point of view of linear stability, dipole solitons

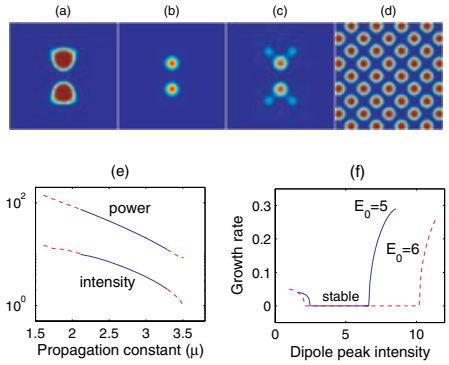

Figure 1. (a)–(c) Diagonal OOP dipole solitons at $E_0 = 6$ and peak intensities 12, 3, and 1, respectively; (d) the lattice field; (e) power and intensity diagrams of these solitons at $E_0 = 6$ (the dashed lines indicate unstable solitons); and (f) growth rates of infinitesimal perturbations on these solitons at $E_0 = 5$ and 6.

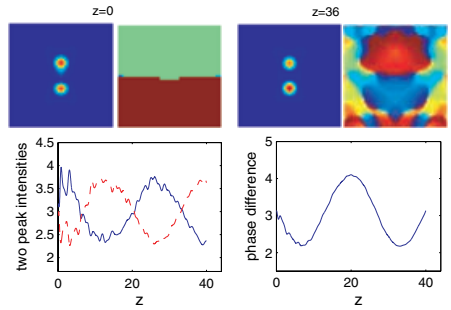

Figure 2. Stable evolution of a diagonal OOP dipole soliton with $E_0 = 6$ and peak intensity $I_p = 3$ (see Figure 1b) under 5% random-noise perturbations. Upper row: intensity and phase fields at $z = 0$ and 36, respectively; lower row: evolutions of peak intensities (left) and phase difference (right) of the two humps.

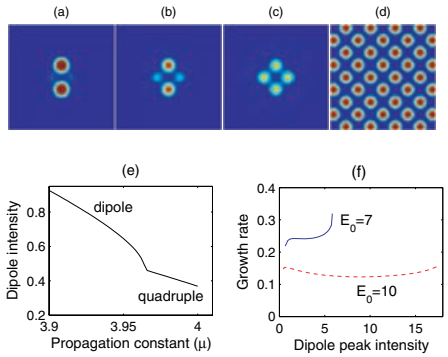

Figure 3. (a, b) Diagonal IP dipole solitons at $E_0 = 7$ and peak intensities 3 and 1, respectively; (c) a quadrupole soliton at peak intensity 0.4; (d) the lattice field; (e) intensity diagram of these solitons at $E_0 = 7$; and (f) growth-rates of infinitesimal perturbations on these solitons at $E_0 = 7$ and 10.

in this short interval of increasing power are linearly unstable according to the Vakhitov and Kolokolov (VK) criterion [32]. The VK instability is purely exponential, i.e., the eigenvalue is purely real. But since this interval of VK instability is so short for diagonal OOP dipole solitons, and another (oscillatory) instability also exists not only inside this short interval but also beyond (see Figure 1(f)), we will not pay much attention to this interval of VK instability in the remainder of the paper. A similar situation occurs for the nondiagonal dipole solitons as well as OOP quadrupole solitons (see Sections 3 and 4).

An interesting fact in Figure 1(e) is that the intensities of these dipole solitons cannot get arbitrarily low. Indeed, these dipole solitons (at $E_0 = 6$) disappear when their peak intensity $I_p < 0.94$ (i.e., $\mu > 3.51$). Note that the edge of the semiinfinite bandgap (where these solitons reside) at $E_0 = 6$ is $\mu_0 \approx 3.58$. Thus the present dipole solitons do not exist in the interval $3.51 < \mu < \mu_0$. This means that these solitons cannot bifurcate from infinitesimal Bloch waves at the edge of the bandgap. A similar finding has been reported for vortex solitons in a 2D photonic lattice with Kerr nonlinearity [33].

We have also analyzed the linear stability of these dipole solitons by a method as outlined in Section 1. The results for dipole solitons at voltage $E_0 = 6$ are plotted in Figure 1. We see immediately that the diagonal OOP dipole solitons are linearly unstable at high- and low-peak-intensity values. More specifically, when the peak intensity $I_p > 10$ or $I_p < 2.1$, the dipole soliton is linearly unstable. In addition, when $I_p > 10$, the unstable eigenvalue is purely real, thus these solitons suffer a purely exponential instability. While when $I_p < 2.1$, the unstable eigenvalue is complex, thus these solitons suffer an oscillatory instability.

A more important finding in Figure 1 is that in the intermediate intensity regime where $2.1 < I_p < 10$ (for $E_0 = 6$), the diagonal OOP dipole solitons are linearly *stable*. Because critical collapse does not occur in photorefractive crystals (where the nonlinearity is saturable), this linear stability assures nonlinear stability as well. Indeed, we have simulated the nonlinear evolution of the (linearly stable) dipole soliton with $E_0 = 6$ and $I_p = 3$ under random-noise perturbations. The noise has a Gaussian distribution in the spectral k-space with full width at half maximum (FWHM) two times larger than the soliton FWHM spectrum. The noise power is 5% of the soliton's. The simulation result is shown in Figure 2. We see that there is a periodic exchange of energy between the two humps of the dipole, but the soliton does not break up even after 40 z units (corresponding to over 90 mm in physical distances). In addition, the phase structure of the solution remains the same as that of the original dipole. This is evidenced by the phase-field distributions at $z = 0$ and 36 in Figure 2, as well as the lower right figure of Figure 2, which shows that the phase difference between the two humps of the dipole remains close to the initial value π. This simulation, as well as the others we have done for different dipole solitons, shows that when $2.1 < I_p < 10$ (for $E_0 = 6$), OOP

dipole solitons are both linearly and nonlinearly stable. This stability should facilitate the experimental observation of these solitons (as confirmed below).

How does the stability behavior change when the voltage is varied? To answer this question, we have calculated the growth rates of dipole solitons at a different voltage $E_0 = 5$, and the results are plotted also in Figure 1. We see that at this lower voltage, the stability interval is shortened by almost one half to be just $2.5 < I_p < 6.6$. Thus, increasing the voltage significantly stabilizes the OOP dipole solitons.

The OOP dipole solitons are related to lattice-free vector dipole solitons reported before, where one component is a fundamental mode that serves as the waveguide, while the other component is a dipole mode [34–36].

2.2. Diagonal IP dipole solitons

We have also found diagonal IP dipole solitons. Similar to diagonal OOP solitons, these solitons also have two main humps near adjacent diagonal lattice sites, but their phases are constant throughout the entire solution field. At $E_0 = 7$, these solitons exist when $2.9 < \mu < 3.97$, or $0.45 < I_p < 5.86$, and they are shown in Figure 3. In Figures 3(a) and (b), diagonal IP dipole solitons with peak intensities $I_p = 3$ and 1 are displayed (the corresponding propagation constants μ are 3.45 and 3.88). We see that the soliton in Figure 3(a), which has higher intensity, is more localized. The lower-intensity soliton in Figure 3(b), on the other hand, is less localized. In the latter soliton, two satellite lobes appear between the two main humps due to the constructive interference of the main humps. As the intensity of the soliton decreases further, the satellite lobes become more pronounced. When $0 < I_p < 0.45$ (where $3.97 < \mu < 4.08$), these lobes' intensities become equal to the two main humps', thus the dipole solitons become IP quadrupole solitons (which bifurcate from infinitesimal Bloch waves). An IP quadrupole soliton with peak intensity $I_p = 0.4$ (at $\mu = 3.99$) is shown in Figure 3(c). Such solitons will be discussed in more detail in Section 4. We have also calculated the power and intensity diagrams for these solitons, both of which are decreasing functions of μ. The intensity diagram for $E_0 = 7$ is plotted in Figure 3. This diagram clearly shows that diagonal IP dipole solitons smoothly merge into IP quadrupole solitons when their peak intensities $I_p < 0.45$.

Because the power of IP dipole solitons is a decreasing function of μ in its domain of existence, these solitons are free of VK instabilities. However, all these solitons are still linearly unstable. The instability is purely exponential, but not of VK type. For these solitons at $E_0 = 7$, the unstable eigenvalues are displayed in Figure 3. We see that these unstable eigenvalues are all nonzero, meaning that these solitons are all linearly unstable. However, this linear instability can be strongly suppressed if the voltage E_0 is increased. For instance, if $E_0 = 10$, the growth rates of dipole solitons are also shown in

Figure 3. We see that these growth rates at $E_0 = 10$ are much lower than those at $E_0 = 7$. Physically, this suppression of instability at higher voltage occurs because a higher voltage induces a stronger lattice waveguide. In other words, the lattice-induced trapping potential is stronger at higher E_0 values (recall that the lattice-induced change of refractive index δn is proportional to $E_0/(1 + I_l + |U|^2)$). Thus, if the main humps of the soliton are located inside the lattice sites, then higher trapping potential at the lattice sites would suppress their instabilities. In experimental conditions, the crystal length is typically short or moderate (in the range of 6–20 mm). Thus, if this linear instability of IP dipole solitons is sufficiently reduced, then they could still be observed.

In our experiments (to be described later in the text), the input beams are a pair of IP or OOP Gaussian beams. Thus, it is desirable to directly simulate the theoretical model (1) under experimental conditions. For this purpose, we take the crystal length $L = 10$ mm, the lattice spacing $D = 20$ mm, and the lattice peak intensity $I_0 = 3I_d$. The voltage E_0 can be adjusted to various values as is done in our experiments. At the crystal input, we take the initial condition to be a pair of IP or OOP Gaussian beams centered at two adjacent diagonal lattice sites. The peak intensities of both Gaussian beams are 1/6 of the lattice intensity (i.e., $0.5I_d$), and the FWHM of these Gaussian beams are 10 μm. The simulation results for both OOP and IP launching of Gaussian beams are plotted in Figure 4. The first column shows the input intensity field; the second column shows discrete diffraction at low voltage 40 V/mm; the third column shows self-trapping and dipole-soliton formation at high voltage 200 V/mm; and the last column shows the repulsion/attraction of Gaussian beams at high voltage 200 V/mm without the optical lattice. Note that the discrete diffraction patterns of IP and OOP cases (at low voltages) are very different. While light in the OOP case simply tunnels to outer lattice sites along the original orientation, light in the IP case switches its orientation and tunnels out along orthogonal orientations. The reason is that in the IP case, the interference is constructive. Thus, light in orthogonal lattice sites is reinforced and becomes stronger. In the OOP case, it is just the opposite. But in both cases, the beams are trapped to form dipole solitons when the voltage is high. Without the lattice, it is well known that such dipole-mode solitons cannot exist in a self-focusing media, since the two humps would repel each other, as has been demonstrated before [37].

2.3. Experiments

The dipole solitons predicted above have also been observed in our experiment. The experimental setup is illustrated in Figure 5. Similar to the earlier experiments with fundamental and vortex solitons in 2D optically induced lattices [20, 23], our experiments were performed in a photorefractive crystal illuminated by a spatially modulated light beam ($\lambda_0 = 488$ nm) passing through a rotating diffuser and an amplitude mask. The biased photorefractive crystal

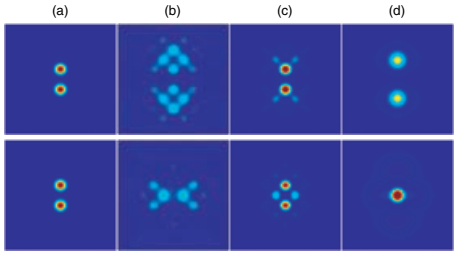

Figure 4. Theoretical results on propagation of two diagonally oriented Gaussian beams in a 10 mm-long crystal with a 2D lattice. Upper row: OOP case; lower row: IP case. From left to right: input; output at low voltage 40 V/mm; output at high voltage 200 V/mm; output at high voltage 200 V/mm without lattice.

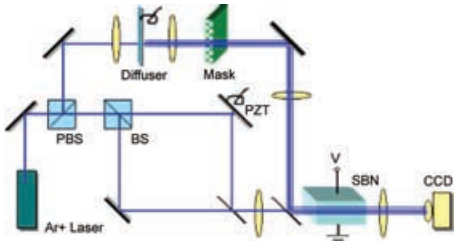

Figure 5. Experimental setup. PBS: polarizing beam splitter; PZT: piezo-transducer; and SBN: strantium barium niobate.

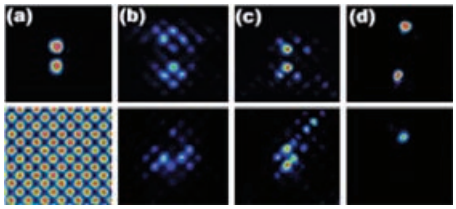

Figure 6. Experimental results on diagonal dipole solitons in a 2D lattice. Top panel: OOP case; bottom panel: IP case. (a) Input; (b) output at a low field of 100 V/mm; (c) and (d) output at a high field of 320 V/mm with and without the lattice. The bottom left shows the lattice pattern.

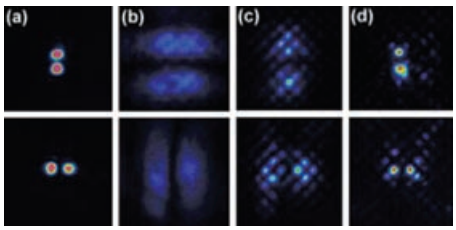

Figure 7. Experimental results on diagonal OOP dipole solitons oriented vertically (top) and horizontally (bottom). (a) Input; (b) linear diffraction at output without the lattice, and (c) discrete diffraction of dipole beam at a bias field of 100 V/mm, and (d) discrete trapping of dipole solitons in the lattice at a higher bias field of 320 V/mm.

(SBN:60, $5 \times 5 \times 8$ mm^3) provides a self-focusing noninstantaneous nonlinearity, and the rotating diffuser makes the beam to be partially spatially incoherent, as was used for the demonstration of incoherent solitons [38]. The amplitude mask provides spatial modulation after the diffuser on the otherwise uniform beam, which exhibits a pixel-like intensity pattern at the input face of the crystal [30]. This pixel-like beam is ordinarily polarized, and is partially coherent as controlled by the rotating diffuser, forming a stable and nearly invariant waveguide lattice in the crystal. In addition, the principal axes of the lattice are oriented in the diagonal directions, as such a lattice will suffer less distortion due to the anisotropic nonlinearity of the crystal. A Gaussian beam split from the same laser output (without passing through the diffuser) is sent into a Mach–Zehnder interferometer. The two extraordinarily polarized beams exiting from the interferometer are used to generate the dipole, and they are combined with the lattice beam before the crystal, propagating collinearly with the lattice beam. Because the dipole beams are coherent and e-polarized while the lattice beam is partially incoherent and o-polarized, the lattice remains nearly invariant under a high bias field, but the dipole itself experiences a strong self-focusing nonlinearity [16]. The relative phase between the two beams for the dipole is tuned with a piezo-transducer (PZT) mirror to be either π (i.e., OOP) or 0 (i.e., IP). The separation between the two beams is adjusted to match the diagonal lattice spacing (about 28 μm). The two beams are launched into two nearby lattice sites in either the vertical or horizontal direction. In addition, a broad incoherent beam is used as background illumination for fine tuning the nonlinearity. The input/output intensity patterns of the dipole and the lattice are monitored with an imaging lens and a CCD camera.

Typical experimental results of dipole lattice solitons are shown in Figure 6, where the top panel is for the OOP dipole and the bottom for the IP dipole. In these experiments, the dipole beams are oriented in the vertical direction. The intensity ratio between the lattice beam and background illumination is about 3, and the intensity of the dipole beam is about six times weaker than that of the lattice. At a low bias field, both types of dipoles undergo linear discrete diffraction in the lattice (Figure 6(b)), exhibiting interesting diffraction patterns similar to those found in our simulations. A clear distinction between the two types of dipoles lies in again the intensity redistribution after discrete diffraction: the intensity for the OOP dipole extends along the original direction of the dipole, while that for the IP dipole extends along the orthogonal direction. Furthermore, due to destructive (constructive) interference, the minimum (maximum) intensity is located in the two sites between the two OOP (IP) dipole lobes. At a high bias field, both types of dipoles are trapped by the lattice potential, leading to the formation of dipole lattice solitons (Figure 6(c)). Note that in the highly nonlinear regime, although some energy is radiated to the lattice sites far away from the dipole, most of the energy is concentrated in the two sites matched by the input dipole. The initial phase structures are

preserved after the lattice dipole solitons are created, as seen from their output intensity patterns (Figure 6(c)). Should one of the dipole beams be turned off, the other forms a fundamental lattice soliton and redistributes the energy to its center as well as four neighboring sites along the principal axes of the lattice. Without the lattice, the dipole diverges in the OOP case and merges into a single soliton in the IP case (Figure 6(d)), as observed previously [37]. In addition to attraction and repulsion, self-bending of the soliton filaments toward crystalline *c*-axis (upward in Figure 6(d)) is evident. This soliton self-bending due to the diffusion effect enhanced by the high bias field is well known [39], and it was not included in our theoretical model for simplicity.

Although both types (OOP and IP) of lattice dipole solitons are observed, we point out that the OOP dipole solitons are stable and robust, and can be generated in either the horizontal or vertical direction with similar dipole structures. Figure 7 shows such a comparison, where (a) is the input of dipole in vertical (top) and horizontal (bottom) directions, (b) is the corresponding diffraction in the linear regime without the lattice potential, (c) is discrete diffraction at a low bias field of 100 V/mm, and (d) is discrete trapping at a higher bias field of 320 V/mm. As seen in Figure 7(d), the OOP dipole soliton keeps the same orientation as in the input. However, the IP dipole-like solitons are less stable, and they can be observed only when oriented vertically at a high bias field. Figure 8 shows the output intensity patterns of the IP dipole as the strength of the nonlinearity is increased when the dipole is launched vertically (top) and horizontally (bottom). Due to constructive interference, the energy of the IP dipole tends to concentrate more at the two sites in the middle of (but orthogonal to) the dipole rather than the two initial input sites (Figures 8(b) and (c)). Furthermore, even at a high bias field, such intensity distribution persists in the horizontally launched dipole (Figures 8(c) and (d)), where the dipole at crystal output shows a 90° "rotation" as compared to the input. In the OOP case, there is no such "rotation" as the light will not tunnel to the sites between the dipole. This anisotropic behavior of self-trapping of IP dipole-like beams is attributed to the anisotropic photorefractive nonlinearity, which has not been fully incorporated in our present theoretical model. Should we launch a train of such IP beams instead of just two beams for the dipole, the anisotropic behavior of discrete diffraction and discrete trapping would become even more evident [20].

3. Dipole solitons in two closest nondiagonal lattice sites

We have also found dipole solitons that are not oriented in the two diagonal lattice sites, but rather, the two humps of the dipole are located at two adjacent lattice sites along the principal axes. The humps can have the same phase or π-phase difference as well. The corresponding solitons will be called IP

and OOP *nondiagonal dipole solitons*, respectively. Even though these dipole solitons share some of the properties of diagonal dipole solitons discussed above, some other properties they exhibit are distinctly different. Below we discuss nondiagonal OOP and IP dipole solitons separately. For these studies, the principal axes of the square lattice are oriented in vertical/horizontal directions, so the dipole solitons will also be in either vertical or horizontal directions (see Figures 9 and 10 for the lattice and dipole orientations).

3.1. Nondiagonal OOP dipole solitons

We have obtained these nondiagonal OOP dipole solitons in a wide parameter region. At $E_0 = 6$, such solitons with peak intensities 7, 4.5, and 1.5 are shown in Figures 9(a)–(c), respectively. The corresponding photonic lattice is displayed in Figure 9(d). As we can see, these solitons are located at two adjacent lattice sites, thus their hump separation is shorter than that in diagonal dipole solitons. At high peak intensity, the two humps are located at the outer skirts of the lattice sites (Figure 9(a)). At moderate intensity, the humps are located almost exactly at the centers of lattice sites (Figure 9(b)). At low intensity, the dipole soliton gets less localized and spreads out to more lattice sites (Figure 9(c)). Due to the destructive interference of the two OOP humps, the light intensity at places between the two humps is zero. This is clearly visible in Figures 9(a)–(c). The power and intensity diagrams of these solitons at $E_0 = 6$ are shown in Figure 9(e). It is seen that the power is a decreasing function of μ (except in the very tiny interval $3.44 < \mu < 3.4406$ at the right end of curves in Figure 9(e) where the power slightly increases). Furthermore, these solitons disappear when $\mu > 3.4406$, or $I_p < 1.4330$. Thus, these solitons cannot bifurcate from infinitesimal Bloch waves at the edge of the bandgap. The linear stability of these solitons at $E_0 = 6$ and a lower value $E_0 = 5.8$ is displayed in Figure 9(f). We see that these solitons are unstable in the higher and lower intensity regimes, but are stable in the intermediate-intensity regime. The instabilities at both the higher and lower intensity regimes are both oscillatory, in contrast with diagonal OOP dipole solitons whose instabilities are purely exponential at high intensities. When the applied field E_0 decreases, the region of stability shrinks. Thus higher applied field stabilizes these solitons.

The properties of nondiagonal OOP dipole solitons listed above are qualitatively similar to those of diagonal OOP dipole solitons in Section 2. But some other properties are distinctly different. First, the discrete-diffraction patterns of nondiagonal OOP solitons are different (cf. Figures 1(c) and 9(c)). While the intensity field in Figure 1(c) spreads out in a "Y" pattern, that in Figure 9(c) spreads out simply along the vertical direction (which is the orientation of the dipole). Another difference is that at the same applied field, the intensity threshold for the existence of OOP dipole solitons is higher for

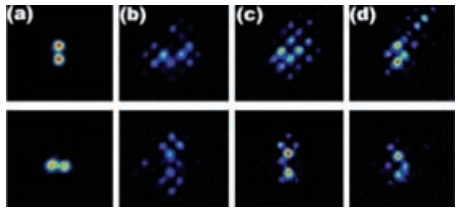

Figure 8. Experimental results on diagonal IP dipoles oriented vertically (top) and horizontally (bottom). (a) Input; (b)–(d) output at a bias field of 100, 260, and 320 V/mm, respectively.

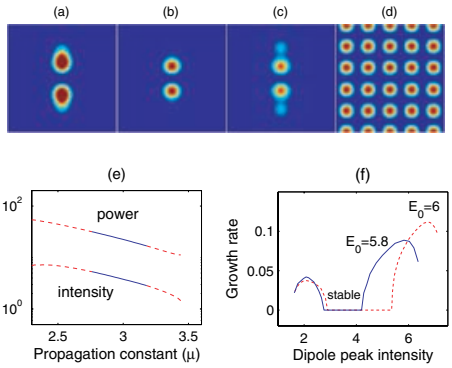

Figure 9. (a)–(c) Nondiagonal OOP dipole solitons at $E_0 = 6$ and peak intensities 7, 4.5, and 1.5, respectively; (d) the lattice field; (e) power and intensity diagrams of these solitons at $E_0 = 6$ (the dashed lines indicate unstable solitons); and (f) growth-rates of infinitesimal perturbations on these solitons at $E_0 = 5.8$ and 6.

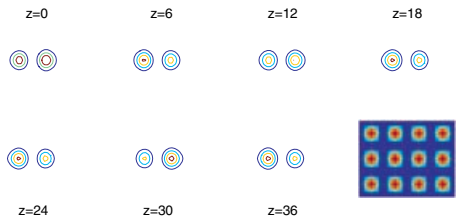

Figure 10. Stable evolution of a nondiagonal OOP dipole soliton with $E_0 = 6$ and peak intensity $I_p = 4.5$ (see Figure 9(b)) under 1% random-noise perturbations. The last figure is the lattice field.

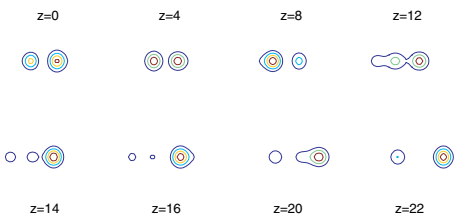

Figure 11. Breakup of the same dipole soliton as in Figure 10 but under stronger (5%) random-noise perturbations.

the nondiagonal case, and lower for the diagonal case. The third difference is that, at the same applied field, the stability region of OOP dipole solitons is larger for the diagonal case, and smaller for the nondiagonal case. In other words, diagonal OOP dipole solitons are more stable than nondiagonal ones. The reasons for the above differences are intimately related to the geometric configurations of these dipole solitons as well as the fact that hump separations of dipoles in the diagonal case are larger than those in the nondiagonal case.

We have also tested the robustness of linearly stable nondiagonal OOP dipole solitons against weak and strong perturbations, and investigated their nonlinear evolutions. We found that under weak perturbations, these solitons undergo internal oscillations and periodically exchange energy between their two humps in a stable fashion. Under stronger perturbations, these solitons can break up. When they break up, interesting tunneling behaviors can be observed as light attempts to escape to different lattice sites. These two evolution scenarios are illustrated in Figures 10 and 11, respectively.

3.2. Nondiagonal IP dipole solitons

As in the case of diagonal dipole solitons, we have also found nondiagonal IP dipole solitons. These solitons at $E_0 = 7$ are shown in Figures 12(a)–(c), where Figure 12(d) shows the lattice field. At moderate peak intensities, these solitons have two main humps that have the same phase and are located at the centers of two adjacent lattice sites (Figure 12(b)). Furthermore, they are quite localized. At lower intensities, the solitons spread to more lattice sites in a way that is distinctly different from nondiagonal OOP dipole solitons (Figure 9(c)). At higher intensities, however, the two humps of the soliton merge together and become a single skewed hump that sits halfway between two adjacent lattices.

Different from other types of dipole solitons discussed above, the present nondiagonal IP dipole solitons continuously merge into infinitesimal Bloch waves as the propagation constant approaches the edge of the semiinfinite bandgap. This can be seen from Figure 12(e), where the intensity diagram at $E_0 = 7$ is displayed. It is seen that the intensity approaches zero when $\mu \to \mu_0 = 4.08$. At lower intensity values, these IP dipole solitons have two main humps (see Figures 12(b) and (c)). At higher intensities, these two humps merge into one (see Figure 12(a)). These facts are labeled in Figure 12(e). We note that near the edge of the bandgap, the envelope of these dipole solitons centers halfway between two adjacent lattice sites. By comparison, the envelope of fundamental lattice solitons centers exactly at a lattice site.

We have studied the power diagram of these solitons as well. We found that the power is a decreasing function of μ, except when μ is quite close to the edge of the bandgap μ_0, where the power increases with μ. This indicates that nondiagonal IP dipole solitons are VK-unstable near the edge of the bandgap, i.e., when the peak intensity is very small.

The nondiagonal IP dipole solitons suffer another purely exponential instability that is not VK type. This instability is stronger, and in addition, it affects all these dipole solitons including those in regions where the power is decreasing with μ (so that the VK instability is absent). To demonstrate this, we have plotted the growth rates of these solitons versus the dipole intensities at $E_0 = 7$ and 10 in Figure 12(f). We see that the growth rates are never zero, so these solitons are all unstable. Note that when $E_0 = 10$, there is an intensity interval $3.38 < I_p < 3.60$ where there exist more than one dipole soliton. This is why there is a cusp in the growth-rate curve in Figure 12(f).

The instability of these dipole solitons at high intensities is easy to understand. Recall that these dipole solitons at high intensities are actually not "dipoles" anymore, as the two humps of the dipoles have merged into a single-hump beam (see Figure 12(a)). More importantly, this single-humped beam sits midway between two adjacent lattice sites, thus they are in an unstable state, just like a particle is sitting at a maximum of the potential. Thus, they are expected to be linearly unstable and tend to break up into several light filaments that move to nearby lattice sites. The above physical reasoning also explains a curious phenomenon in Figure 12(f), where high-intensity dipole solitons are actually more unstable when the applied field E_0 is higher. The reason is that since these solitons are actually single hump and are in an unstable state, when the applied field is higher, it just makes the effective potential steeper, thus making the unstable state to be even more unstable. This contrasts the previous three cases of dipole solitons in Sections 2 and 3, where higher applied field stabilizes them all. When the intensities are moderate where the dipole structure is more pronounced, the higher applied field does suppress linear instabilities as one can see in Figure 12(f).

A mysterious phenomenon in Figure 12(f) is that, when the intensities of these dipole solitons are low, such solitons are again more unstable (with higher growth rates) when the applied field is higher. So far, we do not have a good explanation for it. This issue will be investigated further in the future.

The nondiagonal dipole solitons are interesting due to their different geometric orientations relative to the photonic lattice (compared to diagonal dipole solitons). They also have a smaller hump separation. In addition, under linear propagation, they would exhibit interesting discrete diffraction patterns that are different from diagonal dipoles (see Figure 13). Thus they also make a good object for experimental observations.

To observe nondiagonal dipole solitons in experiments, one can launch two Gaussian beams into adjacent sites along the principal axes of the 2D square lattice. By controlling the relative phase between the initial Gaussian beams, one can observe either IP or nondiagonal OOP dipole solitons. To facilitate potential experiments, we have simulated the propagation of two IP and OOP Gaussian beams launched into two adjacent lattice sites using the model equation (l). For this purpose, we take the crystal length $L = 10$ mm, the

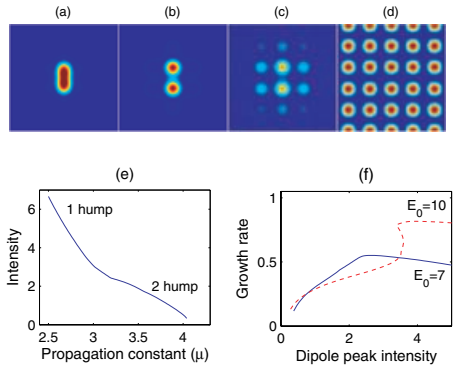

Figure 12. (a)–(c) Nondiagonal IP dipole solitons at $E_0 = 7$ and peak intensities 3, 1, and 0.25, respectively; (d) the lattice field; (e) the intensity diagram of these solitons at $E_0 = 7$; and (f) growth rates of infinitesimal perturbations on these solitons at $E_0 = 7$ and 10.

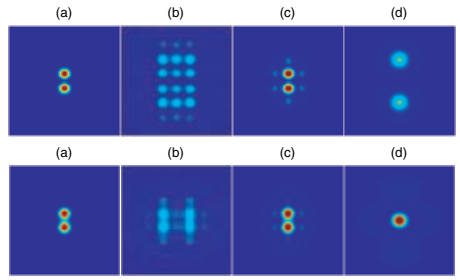

Figure 13. Theoretical results on propagation of two nondiagonally oriented Gaussian beams in a 10 mm-long crystal with a 2D lattice. The lattice field is oriented as in Figures 9(d) and 12(d). Upper row: OOP case; lower row: IP case. From left to right: input; output at low voltage 40 V/mm; output at high voltage 200 V/mm; output at high voltage 200 V/mm without lattice.

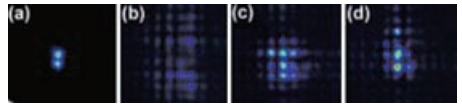

Figure 14. Experimental results on nondiagonal IP dipole solitons located in two closest sites along the principal axes of the lattice. (a) Input and (b)–(d) are the patterns taken at crystal output at bias fields of 90, 200, and 300 V/mm, respectively. The experiments were done in a diagonally oriented lattice as shown in Figure 6(a) (bottom panel). To avoid confusion, the images in this figure have been rotated by 45° so as to be in the same orientation as those from simulations.

nearest-neighbor lattice spacing $D = 20$ mm, the lattice peak intensity $I_0 = 3I_d$, the peak intensities of both Gaussian beams as 1/6 of the lattice intensity (i.e., $0.5I_d$), and the FWHM of these Gaussian beams are 10 μm. The simulation results for both the OOP and IP launching of Gaussian beams are plotted in

Figure 13, and the lattice field is oriented as in Figures 9(d) and 12(d). The first column of Figure 13 shows the input intensity field; the second column shows discrete diffraction at low voltage 40 V/mm; the third column shows self trapping and dipole-soliton formation at high voltage 200 V/mm; and the last column shows the repulsion/attraction of Gaussian beams at high voltage 200 V/mm without the optical lattice. We see that the discrete diffraction patterns of IP and OOP cases (at low voltages) are quite different. While light in the OOP case tunnels primarily along the vertical direction (the direction of the dipole's orientation), light in the IP case tunnels primarily along the horizontal direction. When these diffraction patterns are compared to Figure 4(b) for diagonal dipole solitons, we see that the diagonal or nondiagonal configuration of the dipole makes a big difference on diffraction patterns. However, at a high value of applied voltage, nondiagonal Gaussian beams can also localize and form OOP or IP dipole solitons (see Figure 13(c)), and without the lattice, the Gaussian beams would repel or attract each other. These behaviors are qualitatively the same as diagonal dipole solitons (see Figure 4).

3.3. Experiments

We have also observed the nondiagonal dipole solitons in a 2D square lattice experimentally. The experimental setup is the same as that illustrated in Figure 5, except now that the two beams are launched next to each other along the principal (rather than diagonal) axes of the lattice. The lattice with about 20 μm adjacent-site spacing is created first, and it is diagonally oriented as shown in Figure 6(a) (bottom panel). Then two Gaussian beams from the Mach–Zehnder interferometer are launched into two adjacent lattice sites along the principal axes of the lattice. To be consistent with the theoretical results in Figures 9–13, our experimental images are rotated by 45° when they are presented. With this rotation, the lattice in our experiments looks similar to Figure 9(d). Figure 14 shows a typical example of an IP nondiagonal lattice dipole soliton, where (a) is the input intensity pattern of the dipole beam, and (b)–(d) are the patterns taken at the crystal output at bias fields of 90, 200, and 300 V/mm, respectively. At the high bias field, the dipole beams are trapped very well in the lattice. These results are in good agreement with numerical simulations. Because the two dipole lobes are located next to each other in closest lattice sites, there is no additional lattice site between the dipole to facilitate the "rotation" as in the case of diagonal dipole solitons. Thus, there is no significant difference between OOP and IP nondiagonal dipoles once they form localized states.

4. Quadrupole solitons

In Figure 3(c), we have discovered quadrupole solitons that have four humps at adjacent lattice sites and a constant phase throughout the soliton field. Such

solitons turn out to exist in a large parameter region as well. In addition, we have found quadrupole solitons with π-phase differences between adjacent humps. We will call these two types of quadrupole solitons as IP and OOP, and study them separately.

4.1. OOP quadrupole solitons

These solitons have four main humps located at four adjacent lattice sites in a square configuration. The diagonal humps have the same phase, but the adjacent humps have π-phase difference. The field profiles of these solitons are displayed in Figures 15(a) and (b) at $E_0 = 7$ and peak intensities 4 and 1.3. The soliton in Figure 15(a) is quite localized, and most of the light is concentrated at the four main humps. The soliton in Figure 15(b), on the other hand, is less localized, and a significant portion of the light is at lattice sites outside the four main sites. Without the lattice, these solitons would not have been possible, as the four humps would push each other out.

The power and intensity diagrams of these quadrupole solitons at $E_0 = 7$ have been obtained and shown in Figure 15(c). These diagrams are qualitatively similar to those in Figures 1(e) and 9(e) for diagonal OOP solitons. For instance, there is an intensity threshold below which these solitons do not exist. For $E_0 = 7$, these solitons cannot exist when $I_p < 1.27$, or in terms of the propagation constant μ, when $\mu > 4.05$. Thus OOP quadrupole solitons do not bifurcate from the edge of the bandgap. Another similarity to Figure 1(e) is that, while the power is largely a decreasing function of μ, at the right end of the curves in the diagram, there is a tiny region $4.03 < \mu < 4.05$ where the power slightly increases, signaling the VK instability there.

We have studied the linear stability of these OOP quadrupole solitons as well, and the results at two applied fields $E_0 = 6.5$ and 7 are plotted in Figure 15(d). One can see that OOP quadrupole solitons at high and low intensities are linearly unstable. Furthermore, the leading instabilities in both intensity regimes are oscillatory. However, in the intermediate-intensity region, these solitons are linearly stable. When the applied field increases from $E_0 =$ 6.5 to 7, the stability region expands. Thus higher applied field stabilizes OOP quadrupole solitons. These stability properties resemble those of diagonal and nondiagonal OOP dipole solitons (see Figures 1(f) and 9(f)). Intuitively, OOP quadrupole solitons can be thought of as four nondiagonal OOP dipole solitons linked together. Thus, it is not very surprising that their stability properties are similar to those of nondiagonal OOP dipole solitons.

4.2. IP quadrupole solitons

IP quadrupole solitons have four main humps at adjacent lattice sites, and these humps have the same phase. A typical example is shown in Figure 16(b) where $E_0 = 7$ and the peak intensity is $I_p = 1$. As the intensity of the soliton increases, the four humps merge together into one, and this single-humped

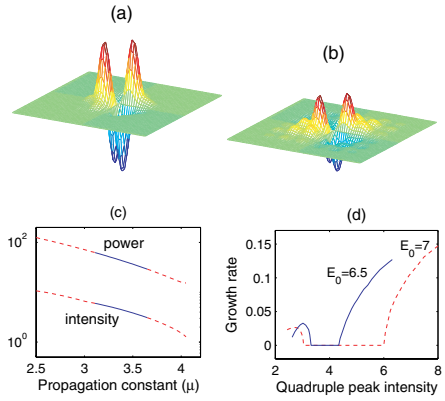

Figure 15. (a, b) Field profiles of OOP quadrupole solitons at $E_0 = 7$ and peak intensities 4 and 1.3, respectively; (c) power and intensity diagrams of these solitons at $E_0 = 7$ (the dashed lines indicate unstable solitons); and (d) growth rates of infinitesimal perturbations on these solitons at $E_0 = 6.5$ and 7.

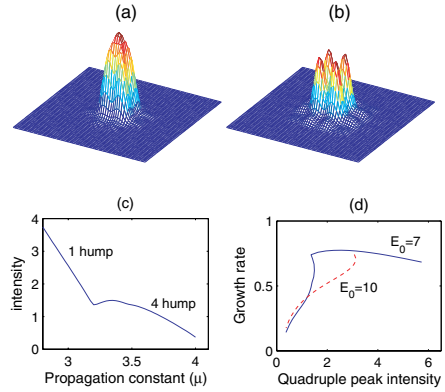

Figure 16. (a, b) Field profiles of IP quadrupole solitons at $E_0 = 7$ and peak intensities 2 and 1, respectively; (c) power and intensity diagrams of these solitons at $E_0 = 7$ (the dashed lines indicate unstable solitons); and (d) growth rates of infinitesimal perturbations on these solitons at $E_0 = 7$ and 10.

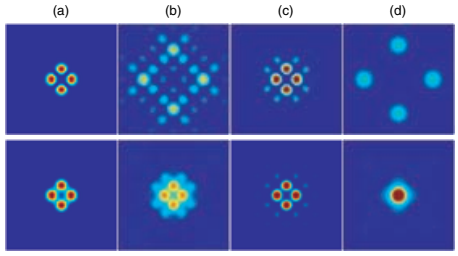

Figure 17. Theoretical results on propagation of four Gaussian beams in a 10 mm-long crystal with a 2D lattice. Upper row: OOP case; lower row: IP case. From left to right: input; output at low voltage 40 V/mm; output at high voltage 200 V/mm; output at high voltage 200 V/mm without lattice.

soliton centers off-site (between four adjacent lattice sites). This can be seen in Figure 16(a), where the IP quadrupole soliton at $E_0 = 7$ and peak intensity $I_p = 2$ is shown. We have obtained the intensity diagram of these solitons at $E_0 = 7$ and plotted it in Figure 16(c). This diagram clearly shows how IP quadrupole solitons with four humps smoothly merge into a single-hump soliton.

IP quadrupole solitons bifurcate from infinitesimal Bloch waves at the edge of the bandgap. This is similar to nondiagonal IP dipole solitons. However, we have found that near the edge of the bandgap, the power of IP quadrupole solitons is a decreasing function of μ, whereas the power of nondiagonal IP dipole solitons is an increasing function of μ. These results will have interesting implications on the linear stability of these solitons near the edge of the bandgap, where a theoretical analysis is possible.

We have also studied the linear stability of these IP quadrupole solitons, and the results are shown in Figure 16(d). This figure indicates that IP quadrupole solitons are always linearly unstable. In addition, we have found that the instability is purely exponential. When the applied field is increased, we find that the instability on IP quadrupole solitons with moderate intensities is reduced, but the instability on solitons with low intensities is actually enhanced. These properties are similar to those in Figure 12(f) for nondiagonal IP dipole solitons.

Both types of quadrupole solitons should be observable in experiments, In fact, our experimental results on IP diagonal dipole solitons already show a structure akin to an IP quadrupole soliton discussed here (see Figure 8(c), top panel). In order to observe both types of quadrupole solitons directly, we can launch four separate Gaussian beams instead of two into the four neighboring lattice sites. The challenge with four beams is to carefully align them with the lattice and control their relative phases to be either the same or with a π difference between neighboring beams. Experiments are currently underway for the creation of OOP quadrupole solitons by phase engineering of a single Gaussian beam. To facilitate experimental observations, we here simulate the propagation of four Gaussian beams in the lattice under low and high voltages and predict what could happen in experiments. For this purpose, we again take the crystal length $L = 10$ mm, the lattice spacing $D = 20$ mm, the lattice peak intensity $I_0 = 3I_d$, the peak intensities of all four Gaussian beams as 1/6 of the lattice intensity (i.e., $0.5I_d$), and the FWHM of these Gaussian beams as 10 μm. The simulation results for both the OOP and IP launching of the four Gaussian beams are plotted in Figure 17. The first column of Figure 17 shows the input intensity field; the second column shows discrete diffraction at low voltage 40 V/mm; the third column shows the self-trapping and quadrupole-soliton formation at high voltage 200 V/mm; and the last column shows the repulsion/attraction of the Gaussian beams at high voltage 200 V/mm without the optical lattice. We see that in the OOP case, the field exhibits interesting discrete-diffraction patterns at the low applied voltage. The light tunnels out rather quickly in square patterns. In the IP case, however, light tunneling to outer lattice sites is much slower. At the high applied voltage, the

Gaussian beams form quadrupole solitons in both the OOP and IP cases (see Figure 17(c)). In addition, the field patterns of the OOP and IP solitons are similar. Without the lattice, the Gaussian beams repel each other in the OOP case and attract each other and coalesce in the IP case, just as expected (see Figure 17(d)).

5. Summary

In summary, we have studied the formation of dipole and quadrupole solitons in 2D photorefractive lattices both theoretically and experimentally. Theoretically, the OOP dipole and quadrupole solitons are shown to be stable in the intermediate-intensity regimes. The IP dipole and quadrupole solitons are linearly unstable, but the instability growth rates can be rather small in the low-intensity region. In addition, high applied voltage can suppress linear instabilities of IP diagonal dipole solitons. Experimentally, we have observed both IP and OOP diagonal and nondiagonal dipole solitons, as well as IP quadrupole solitons. The experimental results agree well with the theoretical results. In addition, we have shown experimentally that the anisotropy of the photorefractive crystal has a significant effect on the formation of IP dipole solitons.

Acknowledgments

This work was supported in part by AFOSR ARO, NASA EPSCoR, NNSF of China, and Research Corp.

References

1. R. Y. Chiao, E. Garmire, and C. H. Townes, Self-trapping of optical beams, *Phys. Rev. Lett.* 13:479 (1964).
2. V. E. Zakharov and A. B. Shabat, Exact theory of two-dimensional self-focusing and one-dimensional self-modulation of waves in nonlinear media, *Sov. Phys. JETP* 34:62–69 (1972).
3. M. Ablowitz and H. Segur, *Solitons and the Inverse Scattering Transforms*, SIAM, Philadelphia, 1981.
4. J. S. Aitchison, A. M. Weiner, Y. Silberberg, M. K. Oliver, J. L. Jackel, D. E. Leaird, E. M. Vogel, and P. W. E. Smith, Observation of spatial optical solitons in a nonlinear glass waveguide, *Opt. Lett.* 15:471 (1990).
5. P. L. Kelley, Self-focusing of optical beams, *Phys. Rev. Lett.* 15:1005 (1965).
6. V. E. Zakharov and A. M. Rubenchik, Instability of waveguides and solitons in nonlinear media. *Sov. Phys. JETP* 38:494 (1974).
7. P. Gunter and J. P. Huignard, eds. *Photorefractive Materials and Applications*, Springer-Verlag, Berlin, 1988.

8. M. Segev, B. Crosignani, A. Yariv, and B. Fischer, Spatial solitons in photorefractive media, *Phys. Rev. Lett.* 68:923 (1992).
9. G. Duree, J. L. Shultz, G. Salamo, M. Segev, A. Yariv, B. Crosignani, P. Di Porto, E. Sharp, and R. Neurgaonkar, Observation of self-trapping of an optical beam due to the photorefractive effect, *Phys. Rev. Lett.* 71:533 (1993).
10. M. Shih, M. Segev, G. C. Valley, G. Salamo, B. Crosignani, and P. Di Porto, Observation of two-dimensional steady-state photorefractive screening solitons, *Electron. Lett.* 31:826 (1995).
11. Z. Chen, M. Mitchell, M. Shih, M. Segev, M. Garrett, and G. Valley, Steady-state dark photorefractive screening-solitons, *Opt. Lett.* 21:629 (1996).
12. D. N. Christodoulides, F. Lederer, and Y. Silberberg, Discretizing light behaviour in linear and nonlinear waveguide lattices, *Nature* 424:817–823 (2003).
13. D. K. Campbell, S. Flach, and Y. S. Kivshar, Localizing energy through nonlinearity and discreteness, *Phys. Today* 57:43–49 (2004).
14. D. Mandelik, H. S. Eisenberg, Y. Silberberg, R. Morandotti, and J. S. Aitchison, Band-gap structure of waveguide arrays and excitation of Floquet–Bloch solitons, *Phys. Rev. Lett.* 90:053902 (2003); R. Morandotti, H. S. Eisenberg, Y. Silberberg, M. Sorel, and J. S. Aitchison, Self-focusing and defocusing in waveguide arrays, *Phys. Rev. Lett.* 86:3296 (2001).
15. N. K. Efremidis, S. Sears, D. N. Christodoulides, J. W. Fleischer, and M. Segev, Discrete solitons in photorefractive optically induced photonic lattices, *Phys. Rev. E* 66:046602 (2002).
16. J. W. Fleischer, T. Carmon, M. Segev, N. K. Efremidis, and D. N. Christodoulides, Observation of discrete solitons in optically induced real time waveguide arrays, *Phys. Rev. Lett.* 90:023902 (2003); J. W. Fleischer, M. Segev, N. K. Efremidis, and D. N. Christodoulides, Observation of two-dimensional discrete solitons in optically induced nonlinear photonic lattices, *Nature* 422:147 (2003).
17. D. Neshev, E. Ostrovskaya, Y. Kivshar, and W. Krolikowski, Spatial solitons in optically induced gratings, *Opt. Lett.* 28:710 (2003).
18. A. A. Sukhorukov, D. Neshev, W. Krolikowski, and Y. S. Kivshar, Nonlinear Bloch–wave interaction and Bragg scattering in optically-induced lattices, www.arxiv/nlin.PS/0309075 (2003).
19. J. Meier, J. Hudock, D. N. Christodoulides, G. Stegeman, Y. Silberberg, R. Morandotti, and J. S. Aitchison, Discrete vector solitons in kerr nonlinear waveguide arrays, *Phys. Rev. Lett.* 91:143907 (2003).
20. H. Martin, E. D. Eugenieva, Z. Chen, and D. N. Christodoulides, Discrete solitons and soliton-induced dislocations in partially-coherent photonic lattices, *Phys. Rev. Lett.* 92:123902 (2004); Z. Chen, H. Martin, E. D. Eugenieva, J. Xu, and A. Bezryadina, Anisotropic enhancement of discrete diffraction and formation of two-dimensional discrete-soliton trains, *Phys. Rev. Lett.* 92:143902 (2004).
21. B. A. Malomed and P. G. Kevrekidis, Discrete vortex solitons, *Phys. Rev. E* 64:026601 (2001).
22. J. Yang and Z. Musslimani, Fundamental and vortex solitons in a two-dimensional optical lattice, *Opt. Lett.* 23:2094 (2003).
23. D. N. Neshev, T. J. Alexander, E. A. Ostrovskaya, Y. S. Kivshar, H. Martin, I. Makasyuk, Z. Chen, Observation of discrete vortex solitons in optically-induced photonic lattices, *Phys. Rev. Lett.* 92:123903 (2004).

24. J. W. Fleischer, G. Bartal, O. Cohen, O. Manela, M. Segev, J. Hudock, and D. N. Christodoulides, Observation of vortex-ring discrete solitons in 2D photonic lattices, *Phys. Rev. Lett.* 92:123904 (2004).
25. J. Yang, Stability of vortex solitons in a photorefractive optical lattice, *New J. Phys.* 6:47 (2004).
26. Z. Chen, I. Makasyuk, A. Bezryadina, and J. Yang, Observation of two-dimensional lattice vector solitons, *Opt. Lett.*, 29, 1656 (2004).
27. P. G. Kevrekidis, A. R. Bishop, and K. Ÿ. Rasmussen, Twisted localized modes, *Phys. Rev. E* 63:036603 (2001).
28. A. A. Sukhorukov and Y. S. Kivshar, Spatial optical solitons in nonlinear photonic crystals, *Phys. Rev. E* 65:036609 (2002).
29. P. G. Kevrekidis, B. A. Malomed, and A. R. Bishop, Bound states of two-dimensional solitons in the discrete nonlinear Schrodinger equation, *J. Phys. A* 34:9615–9629 (2001).
30. Z. Chen and K. McCarthy, Spatial soliton pixels from partially incoherent light, *Opt. Lett.* 27:2019 (2002).
31. V. I. Petviashvili, Equation of an extraordinary soliton, *Plasma Phys.* 2:469 (1976).
32. N. G. Vakhitov and A. A. Kolokolov, *Izy. Vyssh. Uchebn. Zaved. Radiofiz.* 16:1020 (1973) (*Radiophys. Quantum Electron.* 16:783 (1973)).
33. Z. H. Musslimani and J. Yang, Localization of light in a two-dimensional periodic structure, *J. Opt. Soc. Am. B.* 21:973–981 (2004).
34. J. J. García-Ripoll, V. M. Pérez-García, E. A. Ostrovskaya, and Yu. S. Kivshar, Dipole-mode vector solitons, *Phys. Rev. Lett.* 85:82–85 (2000); W. Krolikowski, E. A. Ostrovskaya, C. Weilnau, M. Geisser, G. McCarthy, Yu. S. Kivshar, C. Denz, and B. Luther-Davies, Observation of dipole-mode vector solitons, *Phys. Rev. Lett.* 85:1424–1427 (2000).
35. T. Carmon, C. Anastassiou, S. Lan, D. Kip, Z. H. Musslimani, M. Segev, and D. N. Christodoulides, Observation of two-dimensional multimode solitons, *Opt. Lett.* 25:1113 (2000).
36. J. Yang and D. E. Pelinovsky, Stable vortex and dipole vector solitons in a saturable nonlinear medium, *Phys. Rev. E* 67:016608 (2003).
37. J. S. Aitchison, A. M. Weiner, Y. Silberberg, D. E. Leaird, M. K. Oliver, J. L. Jackel, and P. W. E. Smith, Experimental observation of spatial soliton interactions, *Opt. Lett.* 16:15 (1991).
38. M. Mitchell, Z. Chen, M. Shih, and M. Segev, Self-trapping of partially spatially incoherent light, *Phys. Rev. Lett.* 77:490 (1996); Z. Chen, M. Mitchell, M. Segev, T. H. Coskun, and D. N. Christodoulides, Self-trapping of dark incoherent light beams, *Science* 280:889 (1998).
39. S. R. Singh and D. N. Christodoulides, Evolution of spatial optical solitons in biased photorefractive media under steady state conditions, *Opt. Commun.* 118:569–576 (1995).

University of Vermont
San Francisco State University
Nankai University

(Received May 10, 2004)